HHS Public Access

Author manuscript

Inorg Chem. Author manuscript; available in PMC 2018 November 06.

Published in final edited form as:

Inorg Chem. 2017 November 06; 56(21): 13205–13213. doi:10.1021/acs.inorgchem.7b01945.

Distinguishing Nitro vs Nitrito Coordination in Cytochrome *c*′ Using Vibrational Spectroscopy and Density Functional Theory

Zach N. Nilsson[†,‖], **Brian L. Mandella**[†], **Kakali Sen**[‡,§], **Demet Kekilli**[‡,#], **Michael A Hough**[‡], **Pierre Moenne-Loccoz**[*,⊥], **Richard W. Strange**[*,‡], and **Colin R. Andrew**[*,†]

[†]Department of Chemistry and Biochemistry, Eastern Oregon University, La Grande, Oregon 97850, United States

[‡]School of Biological Sciences, University of Essex, Colchester Essex, CO4 3SQ, United Kingdom

[§]Scientific Computing Department, STFC Daresbury Laboratory, Warrington, Cheshire WA4 4AD, United Kingdom

[⊥]Division of Environmental and Biomolecular Systems, Oregon Health and Science University, Portland, Oregon 97239, United States

Abstract

Nitrite coordination to heme cofactors is a key step in the anaerobic production of the signaling molecule nitric oxide (NO). An ambidentate ligand, nitrite has the potential to coordinate via the N- (nitro) or O- (nitrito) atoms in a manner that can direct its reactivity. Distinguishing nitro vs nitrito coordination, along with the influence of the surrounding protein, is therefore of particular interest. In this study, we probed Fe(III) heme-nitrite coordination in *Alcaligenes xylosoxidans* cytochrome *c*′ (AXCP), an NO carrier that excludes anions in its native state but that readily binds nitrite (K_d ~ 0.5 mM) following a distal Leu16 → Gly mutation to remove distal steric constraints. Room-temperature resonance Raman spectra (407 nm excitation) identify ν(Fe–NO_2), δ(ONO), and ν_s(NO_2) nitrite ligand vibrations in solution. Illumination with 351 nm UV light results in photoconversion to {FeNO}^{6} and {FeNO}^{7} states, enabling FTIR measurements to distinguish ν_s(NO_2) and ν_{as}(NO_2) vibrations from differential spectra. Density functional theory calculations highlight the connections between heme environment, nitrite coordination mode, and vibrational properties and confirm that nitrite binds to L16G AXCP exclusively through the N atom. Efforts to obtain the nitrite complex crystal structure were hampered by photochemistry in the X-ray beam. Although low dose crystal structures could be modeled with a mixed nitrite (nitro)/H_2O distal population, their photosensitivity and partial occupancy underscores the value of

[*]Corresponding Authors: moennelo@ohsu.edu. rstrange@essex.ac.uk. candrew@eou.edu.

[‖]Present Addresses: Z.N.N: Chemistry Department, Colorado State University, Ft. Collins, CO 80523

[#]D.K: Department of Biology and Chemistry, Paul Scherer Institute, CH-5232 Villigen PSI, Switzerland

Supporting Information: The Supporting Information is available free of charge on the ACS Publications website at DOI: 10.1021/acs.inorg-chem.7b01945.

Additional spectroscopic, kinetic, DFT, and structural data (PDF)

ORCID: Pierre Moënne-Loccoz: 0000-0002-7684-7617

Colin R. Andrew: 0000-0001-5908-012X

Notes: The authors declare no competing financial interest.

the vibrational approach. Overall, this study sheds light on steric determinants of hemenitrite binding and provides vibrational benchmarks for future studies of heme protein nitrite reactions.

Graphical abstract

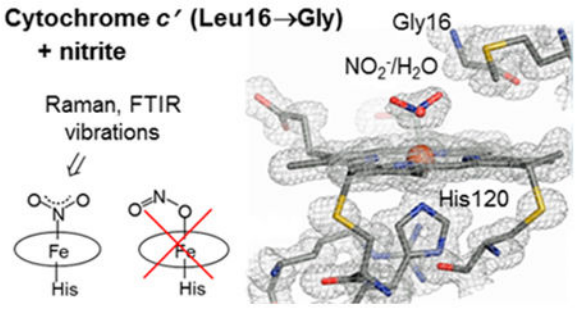

Introduction

Heme proteins are key players in metabolizing nitrite (NO_2^-) to the signaling molecule nitric oxide (NO).[1] Nitrite binding to heme initiates the anaerobic production of NO in proteins such as hemoglobin (Hb), myoglobin (Mb), cytoglobin, neuroglobin, globin X, nitric oxide synthase, nitrophorins, and cytochrome *c* oxidases.[1–5] Within the nitrogen cycle, cytochrome cd_1 nitrite reductase also converts nitrite to NO during denitrification.[6] Although the exact mechanisms of $NO_2^- \rightarrow$ NO conversion as a function of heme protein type (involving nitrite reductase, nitrite anhydrase, or nitrite dismutase activities) remain unresolved, each reaction begins with NO_2^- coordination to the heme Fe.

A characteristic of the nitrite anion is its ability to coordinate via its N- (nitro) or O- (nitrito) atoms (Figure 1). Because N-vs O- coordination is proposed to influence nitrite reactivity,[6–9] establishing the particular Fe-nitrite coordination mode is an important first step in defining structure–reactivity relationships. Examples of η_1-N and η_1-O linkage isomerism have been reported in X-ray crystal structures of nitrite complexes of Fe(III) heme proteins. N atom nitro linkage is observed in crystal structures of heme-containing nitrite reductases[10,11] and nitrophorins,[12,13] whereas the nitrite complex of human Hb[14] and chlorite dismutase[15] exhibit O atom *cis*/*trans*- and *cis*-nitrito modes, respectively. In the case of horse heart Mb, the nitrite coordination mode is sensitive to distal pocket mutations. Removal of distal H-bonding (H64V Mb) changed the nitrite coordination mode from an O atom *trans*-nitrito (wt Mb) to N-bound nitro,[8] and reinserting an H-bonding residue (H64V/V67R Mb) re-established O atom coordination, albeit with a *cis*-like conformation.[8]

Theoretical studies predict that the energy differences between nitro and nitrito isomers of porphyrin complexes can range from ~0 to 40 kJ mol^{-1},[7,9,16–20] and there are reports that the nitrite coordination mode can be affected by sample temperature as well as X-ray-induced photochemistry.[7,21–23] Accordingly, there may be cases in which cryogenic crystal structures do not represent the nitrite coordination mode present under physiological conditions.

The most commonly applied spectroscopic techniques for studying heme-nitrite binding in solution (UV–vis and EPR) detect nitrite coordination indirectly via its effect on the Fe(III) spin state. However, the Fe(III) spin state does not unambiguously define the nitrite linkage isomer. Ford and co-workers have reported examples of nitro and nitrito Fe-porphyrin complexes that are both low spin (LS) with indistinguishable UV–vis absorbance spectra.[17] Moreover, the spin state can vary in response to sample temperature, a case in point being the Fe(III)-nitrite complex of Mb, where cryogenic EPR spectra reveal a high spin (HS) complex but room-temperature UV–vis spectra indicate a mixture of HS and LS species.[23]

A direct means of spectroscopically probing heme-nitrite coordination is via the vibrational frequencies of the Fe-nitrite unit. Experimental frequencies (from RR or FTIR spectroscopy) can be compared with data from model complexes and DFT calculations to distinguish between different nitrite coordination modes. Heme-nitrite vibrations were recently reported for two protein complexes: Mb and horseradish peroxidase (HRP).[24–27] However, in both cases, nitrite undergoes additional reactions with the porphyrin vinyl groups, altering the absorption, spin-state, and vibrational properties. By contrast, *c*-type cytochromes (in which porphyrin vinyl groups are replaced by thioether linkages) are not susceptible to nitrovinyl formation.

Cytochrome *c*′ is a NO-binding *c*-type heme protein found in certain bacteria, including denitrifying, methanotrophic, nitrogen-fixing, and pathogenic organisms.[28] Despite containing mono-His ligated heme, their crowded hydrophobic distal pockets severely hinder coordination with exogenous ligands, even forcing NO to bind to the opposite (proximal) heme face.[29] Replacement of the distal Leu16 residue of *Alcaligenes xylosoxidans* cytochrome *c*′ (AXCP) with Gly or Ala boosts the Fe(II) heme affinities for diatomic gas ligands by a remarkable ~10^6–10^8-fold,[29–31] an effect ascribed to a more accessible distal site as well as ultraefficient geminate recombination.[32] In this study, we harnessed the favorable distal heme reactivity of L16G AXCP to characterize nitrite coordination to the Fe(III) state using spectroscopy (RR, FTIR, UV-visible absorption, and EPR), stopped-flow kinetics, DFT calculations, and X-ray crystallography. Ferric L16G AXCP has a nitrite affinity (K_d ~ 0.5 mM) that is ~20–30-times greater than that of myoglobin despite the absence of distal H-bonding. Vibrations of the Fe(III) nitrite complex were identified using RR and FTIR spectroscopies. In the case of FTIR measurements, assignment of heme-ligand vibrations was facilitated by photoconversion of the nitrite complex to heme-nitrosyl species upon illumination with UV light. Vibrational frequencies and isotope shifts establish that nitrite binds to L16G AXCP via the N (rather than O atom) in solution in agreement with the lowest energy structure from DFT modeling. Nitro coordination was also observed in cryogenic crystal structures of the L16G AXCP nitrite complex, although accompanying X-ray-induced photochemistry underscores the value of vibrational techniques. Overall, this study sheds light on steric determinants of nitrite binding to cytochrome *c*′ and highlights the ability of vibrational spectroscopy to differentiate nitro vs nitrito coordination under physiological conditions.

Experimental Section

Protein Samples, Crystallization, and Reagents

The L16G variant of AXCP was expressed and purified as described previously.[30] Sodium nitrite, including isotopically labeled $Na^{15}NO_2$ (98% ^{15}N, 95% CP) and $Na^{15}N^{18}O_2$ (98% ^{15}N, 95% ^{18}O, 95% CP), was obtained from Sigma-Aldrich. All samples and reagents were prepared in pH 7.0 buffer containing 50 mM MOPS and 0.10 M NaCl. L16G-nitrite AXCP crystals were prepared from the isolated L16G-CO complex,[30] which was oxidized by adding 200 mM (final concentration) of potassium ferricyanide and left at room temperature for 30 min. The sample was run down a PD-10 column to separate the oxidant from the protein. The ferric state was confirmed by UV–vis measurement. Crystallization hanging drops for the L16G AXCP-nitrite complex were set using 20 mg/mL of protein cocrystallized with 50 mM sodium nitrite, 2.2 M ammonium sulfate, and 0.1 M HEPES at pH 7.5. Crystals were transferred for several seconds into cryoprotectant solution (2.2 M ammonium sulfate, 0.1 M HEPES with 40% sucrose) and then stored in liquid nitrogen in preparation for X-ray data collection.

Stopped-Flow Kinetics

Kinetic measurements were conducted at 25.0 °C using an Applied Photophysics SX.18MV-R stopped-flow spectrophotometer (dead time ~1 ms) housed within an anaerobic glovebox (Vacuum Atmospheres Company). Rate constants for nitrite binding were determined by rapidly mixing solutions of ferric L16G AXCP with equal volumes of nitrite solution and monitoring the formation of the nitrite complex with monochromatic light (415 nm) using a photomultiplier detector. Concentrations of nitrite (150–600 μM after mixing) were maintained in >10-fold excess over the heme binding sites (~4 μM heme after mixing) to ensure pseudo-first-order conditions. Pseudo-first-order rate constants, k_{obs}, determined from single exponential fits of time courses, are the average of 3–5 separate kinetic runs. The bimolecular rate constant for nitrite binding (k_{on}) was determined from the slope of the plot of k_{obs} versus nitrite concentration with the nitrite off-rate constant, k_{off}, as the y-intercept. Kinetic measurements conducted in air-saturated buffer gave rate constants similar to those obtained under anaerobic conditions. Illumination of the L16G nitrite complex with the white-light output of the stopped-flow Xe arc lamp resulted in absorption features characteristic of the $\{FeNO\}^6$ species followed by conversion to the $\{FeNO\}^7$ species (200 s total illumination). The UV-light photo-sensitivity of the nitrite complex was used in FTIR measurements to facilitate the identification of heme-ligand vibrations (vide infra).

Spectroscopic Measurements

UV–vis absorption spectra of L16G AXCP solutions containing ~5 μM protein (in heme) were measured using a Cary 60 scanning spectrophotometer. Resonance Raman (RR) measurements of L16G AXCP were conducted on solutions containing ~200 μM (in heme). RR spectra were recorded on a custom McPherson 2061/207 spectrograph (100 μm slit width) equipped with a Princeton Instruments liquid N_2-cooled (LN1100PB) CCD detector. Spectral dispersal was achieved using a 0.67 m focal length and 2400 grooves/mm holographic grating except for measurements of ν(Fe–NO_2) isotope shifts for which a 3600 grooves/mm grating and 1.00 m focal length were used. An excitation wavelength of 406.7

nm was provided by a krypton ion laser, and the Rayleigh line was attenuated using a long-pass filter (RazorEdge, Semrock). Room-temperature RR spectra were collected in a 90° scattering geometry using 7 mW laser power (at the sample) and a reciprocating translation stage. RR spectra of frozen solutions (maintained at 110 K with a liquid nitrogen coldfinger) were collected in an ~150° backscattering geometry with 25 mW laser power at the sample. RR spectra were measured over periods of 3–16 min, using CCl_4, indene, and aspirin standards to calibrate Raman shifts to an accuracy of ±1 cm^{-1}.

FTIR measurements were conducted at room temperature on solutions of the L16G Fe(III) nitrite complex (2 mM in heme). An ~20 μL drop of protein solution was loaded onto the center of a CaF_2 window (International Crystal Laboratories), and a second window was gently placed on top of the droplet to form a film with a 15 μm path length controlled by a Teflon spacer (International Crystal Laboratories). After confirming the integrity of the Fe(III) L16G-nitrite complex via UV–vis absorbance spectra, FTIR spectra were recorded on a Bruker Tensor 27 instrument equipped with a liquid N_2-cooled MCT detector with sets of 1000-scan accumulations at 4 cm^{-1} resolution. The FTIR spectra were collected before and after illumination of the film directly inside the FTIR sample chamber with the 351 nm laser emission of a Krypton laser (Innova 302C, Coherent) for 16 min, which resulted in the appearance of UV-vis absorption features consistent with the formation of $\{FeNO\}^6$ complex (λ_{max} = 419, 530, 564 nm and $\{FeNO\}^7$ (λ_{max} = 416, 541, 574 nm) complexes. Comparison of “dark–illuminated” differential spectra for different nitrite isotopomers enabled identification of Fe(III) nitrite vibrations as positive bands and nitrosyl vibrations as negative bands.

EPR spectra were recorded on a Bruker E-500 X-band EPR spectrometer equipped with a superX microwave bridge and a dual-mode cavity with a helium flow cryostat (ESR900, Oxford Instruments). The protein concentration was 100 μM, and formation of the Fe(III) nitrite complex was confirmed by direct measurement of the visible spectrum in the EPR tube. Samples were frozen in liquid nitrogen and maintained at 10 K during the acquisition of the EPR spectra. The microwave frequency was 9.69 GHz, microwave power 2 mW, modulation frequency 100 kHz, and modulation amplitude 10 G.

Crystallographic Data Collection and Processing

Diffraction data to 1.06 Å resolution were recorded on beamline I04-1 at the Diamond Light Source at 100 K using a Pilatus 6M-F detector and X-ray wavelength 0.92 Å. Images were processed using XDS[33] and Aimless,[34] and the structure was refined and modeled using Remac5[35] and Coot[36] from a starting structure of the native L16G coordinates.[30] Processing and refinement statistics are given in Table S1.

DFT Calculations

These simulations were performed prior to the nitrite complex being obtained experimentally using the crystal structure of L16G-CO AXCP (PDB ID: 2yl3) as a template. The nitrite ligand was modeled at the distal position to Fe(III) heme by coordination to either N or O. The c-heme was modeled as protoporphyrin IX including the propionate groups but discarding the covalently linked Cys residues. His 120 was included in the

proximal position, and the Met 19 residue was included along with Gly 16 to define the distal steric pocket, all residues being truncated at their Cα atoms. The structures were optimized at the DFT level using the B3LYP functional together with the DFT-D3 dispersion correction.[37] The def2-TZVP basis set was used for Fe(III), and def2-SVP[38] was used for all other atoms. A "fragment optimization" protocol within the ORCA package was used for the simulations:[39] the system was divided into several fragments corresponding to the active site residues and heme unit. These individual fragments were internally optimized and pairwise constraints with respect to the distances and orientations between the amino acid fragments and the heme unit were applied during the optimization. The final structures were subjected to frequency calculations at the same level of theory using natural $^{14}N^{16}O_2^-$ and the isotopes $^{15}N^{16}O_2^-$ and $^{15}N^{18}O_2^-$.

Results

Ferric L16G AXCP and Its Reactivity with Nitrite

In contrast to the ferric state of wt AXCP, which retains a 5c heme with no detectable binding of H_2O or anions,[28] the ferric L16G variant exhibits spectroscopic properties indicative of 6c heme with a distal water ligand. Solutions of ferric L16G AXCP (pH 7.0) exhibit a Soret absorption at 405 nm with unresolved α/β bands at ~500 nm and a charge-transfer (CT) high-spin marker absorption at 627 nm (Figure 2, Table S2), whereas porphyrin marker RR vibrations obtained with 407 nm excitation have frequencies characteristic of 6cHS Fe(III) heme (Figure S1, Table S3). Addition of nitrite to ferric L16G AXCP generates a new set of absorbance bands (415, 535, and 571 nm) and porphyrin marker vibrations consistent with a 6cLS hemenitrite complex (Figure 2, Tables S2 and S3).

Low-spin RR marker bands are retained upon cooling to 110 K (Figure S2). EPR spectra obtained at 10 K also indicate the presence of low-spin species with dominant g values consistent with histidine and N-based axial ligand (g_x, g_y, g_z, 1.56, 2.36, 2.84) (Figure S3).[40–42] The nitrite affinity of L16G AXCP, (K_d = 0.50 ± 0.15 mM by titration) is comparable or higher than that of other ferric heme proteins such as Mb (K_d ~ 17 mM) and Hb (K_d ~ 3 mM) (Figure S4, Table S4). Stopped-flow measurements using monochromatic (415 nm) light yield rate constants for nitrite binding, k_{on} (610 ± 30 M^{-1} s^{-1}), and nitrite release, k_{off} (0.41 ± 0.01 s^{-1}) (Figures S5 and S6) with a K_d value calculated from the k_{off}/k_{on} ratio (~0.67 mM) in good agreement with titration measurements (Table S4).

Identification of Fe(III)-Nitrite Vibrations. Vibrations of the L16G Fe(III)NO_2^- unit were identified by RR and FTIR spectroscopy from their frequency downshifts in samples prepared with $^{15}NO_2^-$ or $^{15}N^{18}O_2^-$. Specific vibrational assignments are supported by DFT calculations on energy-minimized structures (described later). RR measurements (407 nm excitation) detect three isotope-sensitive bands in the 300–1400 cm^{-1} region (Figure 3, Figure S7). The RR band at 816 cm^{-1} shifts by −7 cm^{-1} ($^{15}NO_2^-$) and −40 cm^{-1} ($^{15}N^{18}O_2^-$), whereas the 1311 cm^{-1} mode shifts by −21 cm^{-1} ($^{15}NO_2^-$) and −57 cm^{-1} ($^{15}N^{18}O_2^-$) (Table 1). By comparison with FTIR frequencies of sublimed-solid Fe(III)-porphyrin nitro complexes such as Fe(TTP)(NH_3)(NO_2),[41] the 816 cm^{-1} band is ascribed to nitrite ligand bending δ(ONO), and the 1311 cm^{-1} band to the nitrite ligand symmetric stretch, $\nu_s(NO_2)$ (Table 1).

An additional weak RR band observed in the present study at 309 cm^{-1} that exhibits a −2 cm^{-1} shift with $^{15}N^{18}O_2^-$ but no detectable shift with $^{15}NO_2^-$ is suggestive of $FeNO_2$ stretching character ν(Fe–NO_2) (Figure 4, Table 1). Cooling the RR samples to 110 K led to decreased signal quality that precluded the observation of the weaker nitrite ligand modes, although the $^{15}NO_2^-$-sensitive δ(ONO) mode is clearly visible at 815 cm^{-1} (Figure S2). Finally, we note that RR spectra show no evidence of nitrite-derived heme-nitrosyl species based on the absence of N-isotope shifts in the 400–600 cm^{-1} region (Figure S7) that would indicate ν(FeNO) vibrations.[44]

Vibrational assignments complementary to those obtained from RR data were provided by differential FTIR measurements using UV-light sensitivity of the L16G AXCP nitrite complex. Upon exposure to UV light (Xe arc lamp or Kr laser 351 nm line), room-temperature solutions of the L16G nitrite complex exhibited spectroscopic changes consistent with the formation of Fe(III)- and Fe(II)-nitrosyl states (denoted $\{FeNO\}^6$ and $\{FeNO\}$,[7] respectively, to indicate the sum of electrons in metal d and nitrosyl π^* orbitals). A comparison of optical spectra recorded during the photoreaction (Figure S8, bottom panel) with absorption maxima of independently generated L16G AXCP heme species (Figure S8, top panel) suggest that the nitrite complex (415, 536, 569 nm) initially generates the $\{FeNO\}^6$ state (419, 530, 564 nm), which then converts to $\{FeNO\}^7$ (416, 541, 574 nm) (Figure S8). This photochemistry was confirmed and further monitored by FTIR spectroscopy. Accumulation of successive data before and after UV irradiation generated room-temperature photolysis differential FTIR spectra, where vibrations from decaying species are observed as positive bands and negative bands reflect new photogenerated species (Figure 5). A sharp band at 1313 cm^{-1} that decreases upon illumination of unlabeled L16G AXCP-(NO_2^-) and that shifts by −21 cm^{-1} ($^{15}NO_2^-$) and −56 cm^{-1} ($^{15}N^{18}O_2^-$) is readily assigned to the $\nu_s(NO_2)$ mode of the L16G AXCP nitrite ligand observed at 1311 cm^{-1} in the RR (Table 1, Figure 5). A weaker 1396 cm^{-1} FTIR band not identified in the RR spectra shifts by −30 cm^{-1} ($^{15}NO_2^-$) and −62 cm^{-1} ($^{15}N^{18}O_2^-$) and is attributed to the asymmetric stretch of the nitrite ligand, $\nu_{as}(NO_2)$, in agreement with FTIR frequencies of inorganic Fe(III)-porphyrin nitro complexes (Table 1).[43] Another broad feature at ~1230 cm^{-1} that decreases upon illumination and that downshifts by ~13 cm^{-1} ($^{15}NO_2^-$) and ~54 cm^{-1} ($^{15}N^{18}O_2^-$) is consistent with the $\nu_{as}(NO_2)$ mode of free nitrite in aqueous solution (Table 1). In line with trends noted for inorganic nitro complexes,[44] the $\nu_{as}(NO_2)$ frequency of L16G AXCP(NO_2^-) (1396 cm^{-1}) is significantly higher than that of free nitrite (~1240 cm^{-1}), whereas the $\nu_s(NO_2)$ frequencies of L16G AXCP(NO_2^-) (1313 cm^{-1}) and free nitrite are much closer.

As a counterpart to these decreasing FTIR signals, UV irradiation leads to the appearance of new modes consistent with ν(NO) vibrations of heme $\{FeNO\}^6$ and $\{FeNO\}^7$ species. Specifically, a doublet peak at 1902/1915 cm^{-1} that downshifts by 37 cm^{-1} ($^{15}NO_2^-$) and 81 cm^{-1} ($^{15}N^{18}O_2^-$) is attributed to ν(NO) modes of the $\{FeNO\}^6$ complex with minor conformational heterogeneity. In addition, an intense band at 1638 cm^{-1}, which shifts by − 31 cm^{-1} ($^{15}NO_2^-$) and −73 cm^{-1} ($^{15}N^{18}O_2^-$) (Figure 5), is assigned to the ν(NO) mode of the heme $\{FeNO\}^7$ complex in line with RR spectra of $\{FeNO\}^7$ L16G AXCP, which show an isotope-sensitive ν(NO) band at 1630 cm^{-1} shifting by −78 cm^{-1} with $^{15}N^{18}O$ (Figure S9). All other differential FTIR signals show no significant sensitivity to isotopic labeling of

nitrite and are thus assigned to minor porphyrin and protein reorganization upon conversion of the ferric heme-nitro complex to the heme $\{FeNO\}^6$ and $\{FeNO\}^7$ species.

Because the reported photochemistry was not observed with visible light (Kr laser 407 nm and UV-free Xe arc lamp) and was also precluded in samples maintained at cryogenic temperatures, we propose that the conversion of the heme-nitrite complex to the $\{FeNO\}^6$ species depends on bimolecular reactions with photolysis products from free nitrite in solution. The photochemistry of nitrite in water upon excitation within its intense n → π^* transition at 354 nm (ε = 22.7 M^{-1} cm^{-1}) is well-documented and known to produce NO and hydroxyl radicals.[50,51] Rapid radical reactions with free nitrite typically lead to no net reaction (eqs 1–4), but in the presence of L16G AXCP, photogenerated NO and NO_2 radicals may react to form the $\{FeNO\}^6$ species before further reduction to the $\{FeNO\}^7$ state through additional photochemistry and/or reductive nitrosylation.

$$NO_2^- + H_2O + h\nu \rightarrow NO + OH + OH^- \quad (1)$$

$$OH + NO_2^- \rightarrow NO_2 + OH^- \quad (2)$$

$$NO + NO_2 \rightarrow N_2O_3 \quad (3)$$

$$N_2O_3 + H_2O \rightarrow 2NO_2^- + H^+ \quad (4)$$

DFT Calculations

The issue of nitro vs nitrito coordination in L16G AXCP was also investigated by DFT. Calculations were performed using the heme environment from the L16G-CO AXCP crystal structure (PDB ID: 2YL3) as a template and replacing CO with either N- or O-bound nitrite (Figure S10). The optimized geometries of both models (Figure 6A and B) are close to that of the starting crystal structure with the N-coordinated nitrite being lower in energy than the O-bound by 31.5 kJ mol^{-1} (for energies, see Figure S10) in line with N-bound nitrite as the experimentally observed species (confirmed by RR spectroscopy).

Both N- and O-bound forms have their heme propionates oriented toward the distal side (resembling the starting crystal structure), and N-bound nitrite remained the preferred mode in alternative models with either one or both propionates flipped to the proximal side. The symmetrically bound nitro ligand (Figure 6A) has a calculated Fe–N (nitro) distance of 1.94 Å and O–N–O angle of ~123° with sufficient space in the distal pocket to bind to Fe without perturbing the M19 residue, which lies ~4.7 Å from the Fe. By contrast, the higher-energy nitrito complex (Figure 6B) acquires a monodentate *cis* Fe(ONO) orientation (Fe-O bond

length ~1.9 Å, and O–N–O angle ~118°) that is more constrained in its position in the heme pocket by both the M19 and G16 residues.

Vibrational modes of the DFT-optimized structures are shown in Figure S11 with frequencies summarized in Table 1. The N-bound model gives the best agreement with experimental data. Although the calculated vibrational frequencies for the nitro ligand are somewhat higher than those of the experimental values, there is good agreement with the observed pattern of isotope shifts (Table 1). The predicted frequency and $^{15}NO_2^-/^{15}N^{18}O_2^-$ isotope shifts for the ν(Fe–NO_2) mode (309, ~0/−1 cm^{-1}) correspond well with observed values (318, ~0/−2 cm^{-1}) (Table 1). Similarly, for the $\delta(NO_2)$ vibration, the calculated frequency and isotope dependence (849, ~8/−43 cm^{-1}) agree well with experiment (816, ~7/-40 cm^{-1}), whereas calculated frequencies for $\nu_s(NO_2)$ (1428, −23/−65 cm^{-1}) and $\nu_{as}(NO_2)$ (1588, −31/−69 cm^{-1}) compare to observed values of (1311, −21/−57 cm^{-1}) and (1396, −30/−62 cm^{-1}), respectively (Table 1). By contrast, the O-bound model results in poorer agreement with experimental values (Table 1). Most strikingly, the predicted frequencies and $^{15}NO_2^-/^{15}N^{18}O_2^-$ isotope shifts for the nitrito stretching modes, ν(N=O) (1608, −20/−73 cm^{-1}) and ν(N–O) (1094, −22/−47 cm^{-1}) do not correspond well with either of the observed nitro ligand stretches (vide infra), and predicted frequencies for bending mode δ(ONO) (886, −4/−48 cm^{-1}) show a poorer match with experiment than $\delta(NO_2)$ from the nitro model (vide infra).

X-ray Crystal Structure of the L16G AXCP Nitrite Complex

Ferric state L16G crystals grown in the presence of nitrite were used for structure determination. High doses of X-rays (0.78 MGy) led to loss of bound nitrite and observation of ambiguous electron density in the distal heme pocket, consistent with reduction to the Fe(II) state where nitrite does not bind. Attenuation of the beam allowed us to determine a low-dose (0.16 MGy) crystallographic data set at 1.06 Å resolution (Table S1), capturing the ferric state before full reduction of the heme site by the X-rays occurred. The tertiary structure was found to be identical (rmsd < 0.2 Å) to that of nitrite-free L16G AXCP,[30] and the electron density at the Fe-heme site showed that a ligand larger than water was present.

The atomic resolution of the data allowed us to successfully model a mixture of a nitro-coordinated nitrite with Fe-N distance 2.1 Å and a water molecule at 2.07 Å (Figure 7) in the proportion ~1:3. The Fe-N(His) distance is 2.04 Å. The nitrite is located in the distal heme pocket with its O1 atom oriented toward and 3.3 Å away from the Met19Sδ atom and 3.1 Å from the Gly16Cα atom. Measurement of data sets with higher X-ray doses revealed gradual loss of the nitrite ligand and a structure best modeled by a single water molecule coordinated to Fe(II) heme at 2.08 Å with Fe-N(His) at 2.07 Å. While unusual, it is noted that a putative Fe(II)-OH_2 complex (Fe-O distance of 2.17 Å) was recently reported for the chemically reduced state of the L16A variant of AXCP.[29] Although we were able to model N-bound (nitro) coordination in low-dose structures (in agreement with our vibrational and DFT data), the X-ray sensitivity of the Fe(III) nitrite-bound crystals highlights the need for structural characterization using alternate (vibrational) techniques (vide supra).

Discussion

Vibrational Identification of Nitro Coordination

We report the first vibrational and DFT analysis of a *c*-type heme protein nitrite complex Observed vibrational frequencies for the L16G AXCP Fe(III)-nitrite unit are in excellent agreement with previous FTIR data for Fe(III)-nitro porphyrin complexes with nitrogenous base proximal ligands (Table 1).[46] Defining frequencies of these complexes include $\nu_{as}(NO_2)$ ~ 1395–1406 cm^{-1}, $\nu_s(NO_2)$ ~ 1306–1312 cm^{-1}, and $\delta(NO_2)$ ~ 810–816 cm^{-1}. RR spectra of L16G AXCP also identify the $\nu(Fe–NO_2)$ vibration at 309 cm^{-1}. Vibrational assignments are supported by DFT calculations on L16G AXCP, which despite over-estimating the absolute frequencies reproduce the NO_2^- and $^{15}N^{18}O_2^-$ isotope shifts quite well.

In contrast to nitro complexes, monodentate nitrito complexes break the conjugation of the N–O bonds, leading to one N–O stretch at higher energy (corresponding at N=O) and another N–O stretch at lower energy (corresponding to N–O). Such behavior has been previously reported for complexes of Co(III) and Cr(III) [45,52] as well as for Cu(II)-tris(pyrazolyl)methane[53] and Fe(III)(TTP)(NH_3).[46] In the latter case, the nitrito isomer is clearly distinguished from its nitro isomer by the existence of a ν(N=O) mode at 1470 cm^{-1} (higher than the $\nu_{as}(NO_2)$ nitro frequency) and a ν(N–O) mode at 969 cm^{-1}(lower than the nitro $\nu_s(NO_2)$ frequency) (Table 1). The nitrito ligand bending frequency (~827 cm^{-1}) is also slightly higher than that of the nitro counterpart (~810 cm^{-1}). Our DFT calculations on N- vs O-bound models for L16G AXCP reveal the same distinguishing vibrational trends as described above (albeit with higher absolute frequencies) while also predicting that the ν(Fe–ONO) frequency is slightly higher than that of the nitro isomer ν(Fe–NO_2) mode (Table 1).

To our knowledge, the present RR and FTIR data for L16G AXCP contain the first vibrational frequencies of nitrite bound to an Fe(III) heme protein without accompanying porphyrin (vinyl) nitration. Very recently, RR spectra were reported for Fe(III) Mb[24–26] and HRP[27] incubated for extended periods with nitrite. It has been shown that these conditions lead to nitration of the porphyrin 2-vinyl group (Mb) or the 4-vinyl group (HRP).[54,55] This so-called “nitriheme” is the basis of the green coloration in cured meat upon prolonged exposure to excess nitrite under acidic conditions. Mb incubated with 50 mM nitrite leads to the formation of a 6cHS Fe(III) heme nitrito complex (λ_{max} 410 nm) and, upon prolonged incubation,to a 6cLS heme nitrito/nitrovinyl complex (λ_{max} 450 nm).[24,25] Consistent with nitrito coordination, RR spectra of Mb nitrite complex identified a ν(N=O) frequency (1470 cm^{-1}) although bands assigned to ν(N–O) and δ(ONO) exhibited somewhat different frequencies and/or isotope shifts compared to those of Fe(TTP)(NH_3)(ONO) (Table 1).

In the case of Fe(III) HRP,[27] incubation with 50 mM nitrite at pH 7.5 for 3 h led to the generation of a nitrovinyl porphyrin species with a $\nu_s(NO_2)$ RR band at 1334 cm^{-1} but no nitrite coordination to the heme Fe. Upon lowering the pH to 5.5, additional RR frequencies consistent with a low spin Fe(III) heme complex were observed, including several vibrations assigned to a heme-bound nitro complex The $\nu_s(NO_2)$ of Fe(III)-nitro-HRP was assigned at 1272 cm^{-1} on the basis of its isotope shifts with $^{15}N^{16}O_2^-$ (−32 cm^{-1}) and $^{15}N^{18}O_2^-$ (−54

cm^{-1}). Two other bands at 822 and 563 cm^{-1} were assigned to $\delta(NO_2)$ and ν(Fe-NO_2), respectively, based on their nitrite-isotope sensitivity. Although the $\delta(NO_2)$ mode of HRP (822 cm^{-1}) corresponds well to that of Fe(III)NO_2^- L16G AXCP (816 cm^{-1}) (including similar isotope dependence), other vibrations are quite different (Table 1). In particular, the $\nu_s(NO_2)$ mode of HRP (1272 cm^{-1}) is 39 cm^{-1} lower than that of L16G AXCP, and the purported ν(Fe-NO_2) frequency of HRP (563 cm^{-1}) is significantly higher than that of L16G AXCP (309 cm^{-1}) and exhibits much larger $^{15}NO_2^-/^{15}N^{18}O_2^-$isotope shifts (−19/-23 cm^{-1}) than those of L16G AXCP (~0/−2 cm^{-1}). Although the origin of these discrepancies is unclear, they highlight the need for reliable benchmark frequencies for heme-nitrite complexes.

Determinants and Consequences of Nitro vs Nitrito Coordination

The present study highlights the role of steric factors in controlling heme protein-nitrite interactions. Native AXCP has a sterically crowded and hydrophobic distal pocket that limits exogenous ligand binding to weakly bound CO and NO complexes. Removal of steric hindrance via the Leu16 → Gly mutation not only dramatically boosts the affinity for diatomic gases [29,30] but also expands the repertoire of accessible ligands to include the triatomic NO_2^- anion. Our DFT calculations on L16G AXCP predict that N-bound nitrite is energetically favored over O-bound with additional N vs O selectivity possibly arising from steric interactions with Met19.

There appears to be some connection between H-bond stabilization and the nitrite coordination mode. A common feature of heme proteins that exhibit O-bound nitrite (Mb, Hb, chlorite dismutase) is the presence of distal pocket H-bond donors. It is possible that distal H-bonding to nitrite lowers $k_{off}(NO_2^-)$ and that this is reflected in a relatively low $k_{off}(NO_2^-)/k_{off}(CO)$ ratio (because heme-CO complexes are not stabilized significantly by H-bonding).[56] Indeed, the $k_{off}(NO_2^-)/k_{off}(CO)$ ratio for Mb (~140) is ~400-fold lower than for L16G AXCP (~5.5×10^4) (which lacks distal H-bonding residues). Nevertheless, the present study underscores the need for nitro vs nitrito coordination to also be taken into account when interpreting heme-nitrite reactivity trends.

Summary

Using vibrational spectroscopy (RR and FTIR), DFT calculations, and X-ray crystallography, we show that a distal pocket L16G variant of cytochrome c' coordinates nitrite via N-bound (nitro) mode across a range of sample conditions. In particular, the present study highlights the importance of vibrational spectroscopy in distinguishing N- vs O-bound nitrite under physiological conditions, providing a foundation for future characterization of biological heme-nitrite chemistry.

Supplementary Material

Refer to Web version on PubMed Central for supplementary material.

Acknowledgments

This work was supported by the National Science Foundation (MCB-1411963 grant to C.R.A.), BBSRC (award BB/M020924/1 to R.W.S., supporting K.S.), the National Institutes of Health (GM74785 to P.M.-L.), and the Leverhulme Trust (Project Grant RPG2014-355 to M.H. and R.W.S., supporting D.K.). The authors thank McKenzie Evans for help with initial experiments. We thank the Molecular Biophysics Group at the University of Liverpool UK for protocols for preparing the L16G variant.

References

1. Kim-Shapiro DB, Gladwin MT. Mechanisms of nitrite bioactivation. Nitric Oxide. 2014; 38:58–68. [PubMed: 24315961]
2. Li H, Hemann C, Abdelghany TM, El-Mahdy M, Zweier JL. Characterization of the mechanism and magnitude of cytoglobin-mediated nitrite reduction and nitric oxide generation under anaerobic conditions. J Biol Chem. 2012; 287:36623–36633. [PubMed: 22896706]
3. Petersen MG, Dewilde S, Fago A. Reactions of ferrous neuroglobin and cytoglobin with nitrite under anaerobic conditions. J Inorg Biochem. 2008; 102:1777–1782. [PubMed: 18599123]
4. Corti P, Xue J, Tejero J, Wajih N, Sun M, Stolz DB, Tsang M, Kim-Shapiro DB, Gladwin MT. Globin X is a six-coordinate globin that reduces nitrite to nitric oxide in fish red blood cells. Proc Natl Acad Sci U S A. 2016; 113:8538–8543. [PubMed: 27407144]
5. Loullis A, Noor MR, Soulimane T, Pinakoulaki E. The structure of a ferrous heme-nitro species in the binuclear heme a3/CuB center of ba3-cytochrome c oxidase as determined by resonance Raman spectroscopy. Chem Commun. 2015; 51:286–289.
6. Averill BA. Dissimilatory nitrite and nitric oxide reductases. Chem Rev. 1996; 96:2951–2964. [PubMed: 11848847]
7. Silaghi-Dumitrescu R. Linkage isomerism in nitrite reduction by cytochrome cd1 nitrite reductase. Inorg Chem. 2004; 43:3715–3718. [PubMed: 15180427]
8. Yi J, Heinecke J, Tan H, Ford PC, Richter-Addo GB. The distal pocket histidine residue in horse heart myoglobin directs the O-binding mode of nitrite to the heme iron. J Am Chem Soc. 2009; 131:18119–18128. [PubMed: 19924902]
9. Berto TC, Lehnert N. Density functional theory modeling of the proposed nitrite anhydrase function of hemoglobin in hypoxia sensing. Inorg Chem. 2011; 50:7361–7363. [PubMed: 21744811]
10. Williams PA, Fulop F, Garman EF, Saunders NFW, Ferguson SJ, Hajdu J. Haem-ligand switching during catalysis in crystals of a nitrogen-cycle enzyme. Nature. 1997; 389:406–412. [PubMed: 9311786]
11. Lukat P, Rudolf M, Stach P, Messerschmidt A, Kroneck PMH, Simon J, Einsle O. Binding and reduction of sulfite by cytochrome c nitrite reductase. Biochemistry. 2008; 47:2080–2086. [PubMed: 18201106]
12. He C, Ogata H, Knipp M. Formation of the complex of nitrite with the ferriheme b beta-barrel proteins nitrophorin 4 and nitrophorin 7. Biochemistry. 2010; 49:5841–5851. [PubMed: 20524697]
13. He C, Ogata H, Knipp M. Insertion of an H-bonding residue into the distal pocket of the ferriheme protein nitrophorin 4: effect on nitrite-iron coordination and nitrite disproportionation. Chem Biodiversity. 2012; 9:1761–1775.
14. Yi J, Safo MK, Richter-Addo GB. The nitrite anion binds to human hemoglobin via the uncommon O-nitrito mode. Biochemistry. 2008; 47:8247–8249. [PubMed: 18630930]
15. Goblirsch BR, Streit BR, DuBois JL, Wilmot CM. Structural features promoting dioxygen production by Dechloromonas aromatica chlorite dismutase. J Biol Inorg Chem. 2010; 15:879–888. [PubMed: 20386942]
16. Novozhilova IV, Coppens P, Lee J, Richter-Addo GB, Bagley KA. Experimental and density functional theoretical investigations of linkage isomerism in six-coordinate $\{FeNO\}^6$ iron porphyrins with axial nitrosyl and nitro ligands. J Am Chem Soc. 2006; 128:2093–2104. [PubMed: 16464112]

17. Kurtikyan TS, Hovhannisyan AA, Hakobyan ME, Patterson JC, Iretskii A, Ford PC. Reactions of nitrogen oxides with five-coordinate FeIII(porphyrin) nitrito intermediate Fe(Por)-(ONO) in sublimed solids. J Am Chem Soc. 2007; 129:3576–3585. [PubMed: 17338521]

18. Perissinotti LL, Marti MA, Doctorovich F, Luque FJ, Estrin DA. A microscopic study of the deoxyhemoglobin-catalyzed generation of nitric oxide from nitrite anion. Biochemistry. 2008; 47:9793–9802. [PubMed: 18717599]

19. Hopmann KH, Cardey B, Gladwin MT, Kim-Shapiro DB, Ghosh A. Hemoglobin as a nitrite anhydrase: modeling methemoglobin-mediated N_2O_3 formation. Chem - Eur J. 2011; 17:6348–6358. [PubMed: 21590821]

20. Xu N, Yi J, Richter-Addo GB. Linkage isomerization in heme-NOx compounds: understanding NO, nitrite, and hyponitrite interactions with iron porphyrins. Inorg Chem. 2010; 49:6253–6266. [PubMed: 20666385]

21. Trofimov AA, Polyakov KM, Boyko KM, Tikhonova TV, Safonova TN, Tikhonov AV, Popov AN, Popov VO. Structures of complexes of octahaem cytochrome *c* nitrite reductase from Thioalkalivibrio nitratireducens with sulfite and cyanide. Acta Crystallogr, Sect D: Biol Crystallogr. 2010; 66:1043–1047. [PubMed: 20944237]

22. Yi J, Orville AM, Skinner JM, Skinner MJ, Richter-Addo GB. Synchrotron X-ray-induced photoreduction of ferric myoglobin nitrite crystals gives the ferrous derivative with retention of the O-bonded nitrite ligand. Biochemistry. 2010; 49:5969–5971. [PubMed: 20568729]

23. Silaghi-Dumitrescu R, Svistunenko DA, Cioloboc D, Bischin C, Scurtu F, Cooper CE. Nitrite binding to globins: linkage isomerism, EPR silence and reductive chemistry. Nitric Oxide. 2014; 42:32–39. [PubMed: 25172022]

24. Lambrou A, Pinakoulaki E. Resonance Raman detection of the myoglobin nitrito heme Fe-O-N=O/2-nitrovinyl species: implications for helix E-helix F interactions. Phys Chem Chem Phys. 2015; 17:3841–3849. [PubMed: 25562073]

25. Lambrou A, Ioannou A, Pinakoulaki E. Spin crossover in nitrito-myoglobin as revealed by resonance Raman spectroscopy. Chem - Eur J. 2016; 22:12176–12180. [PubMed: 27417111]

26. Ioannou A, Lambrou A, Daskalakis V, Pinakoulaki E. Nitrite coordination in myoglobin. J Inorg Biochem. 2017; 166:49–54. [PubMed: 27815981]

27. Ioannou A, Pinakoulaki E. Probing nitrite coordination in horseradish peroxidase by resonance Raman spectroscopy: Detection of two binding sites. J Inorg Biochem. 2017; 169:79–85. [PubMed: 28160625]

28. Hough MA, Andrew CR. Cytochromes *c′* Structure, reactivity and relevance to haem-based gas sensing. Adv Microb Physiol. 2015; 67:1–84. [PubMed: 26616515]

29. Kekilli D, Petersen CA, Pixton DA, Ghafoor DD, Abdullah GH, Dworkowski FSN, Wilson MT, Heyes DJ, Hardman SJO, Murphy LM, Strange RW, Scrutton NS, Andrew CR, Hough MA. Engineering proximal vs. distal heme-NO coordination via dinitrosyl dynamics: implications for NO sensor design. Chem Sci. 2017; 8:1986–1994. [PubMed: 28451315]

30. Antonyuk SV, Rustage N, Petersen CA, Arnst JL, Heyes DJ, Sharma R, Berry NG, Scrutton NS, Eady RR, Andrew CR, Hasnain SS. Carbon monoxide poisoning is prevented by the energy costs of conformational changes in gas-binding haemproteins. Proc Natl Acad Sci U S A. 2011; 108:15780–15785. [PubMed: 21900609]

31. Garton EM, Pixton DA, Petersen CA, Eady RR, Hasnain SS, Andrew CR. A distal pocket Leu residue inhibits the binding of O_2 and NO at the distal heme site of cytochrome *c′*. J Am Chem Soc. 2012; 134:1461–1463. [PubMed: 22239663]

32. Andrew CR, Petrova ON, Lamarre I, Lambry JC, Rappaport F, Negrerie M. The dynamics behind the affinity: controling heme-gas affinity via geminate recombination and heme propionate conformation in the NO-carrier cytochrome *c′*. ACS Chem Biol. 2016; 11:3191–3201. [PubMed: 27709886]

33. Kabsch W. Xds Acta Crystallogr, Sect D: Biol Crystallogr. 2010; 66:125–132.

34. Evans PR, Murshudov GN. How good are my data and what is the resolution? Acta Crystallogr, Sect D: Biol Crystallogr. 2013; 69:1204–1214. [PubMed: 23793146]

35. Murshudov GN, Skubak P, Lebedev AA, Pannu NS, Steiner RA, Nicholls RA, Winn MD, Long F, Vagin AA. REFMAC5 for the refinement of macromolecular crystal structures. Acta Crystallogr, Sect D: Biol Crystallogr. 2011; 67:355–367. [PubMed: 21460454]
36. Emsley P, Lohkamp B, Scott WG, Cowtan K. Features and development of Coot. Acta Crystallogr, Sect D: Biol Crystallogr. 2010; 66:486–501. [PubMed: 20383002]
37. Grimme S, Antony J, Ehrlich S, Krieg H. A consistent and accurate ab initio parametrization of density functional dispersion correction (DFT-D) for the 94 elements H-Pu. J Chem Phys. 2010; 132:154104. [PubMed: 20423165]
38. Weigend F, Ahlrichs R. Balanced basis sets of split valence, triple zeta valence and quadruple zeta valence quality for H to Rn: Design and assessment of accuracy. Phys Chem Chem Phys. 2005; 7:3297–3305. [PubMed: 16240044]
39. Neese F. The ORCA program system. WIREs Comput Mol Sci. 2012; 2:73–78.
40. Blumberg WE, Peisach J. The low-spin compounds of heme proteins. Adv Chem Ser. 1971; 100:271–291.
41. Taylor CP. The EPR of low-spin heme complexes. Relation of the t2g hole model to the directional properties of the g tensor, and a new method for calculating the ligand field parameters. Biochim Biophys Acta, Protein Struct. 1977; 491:137–148.
42. Young LJ, Siegel LM. On the reaction of ferric heme proteins with nitrite and sulfite. Biochemistry. 1988; 27:2790–2800. [PubMed: 2840947]
43. Kurtikyan TS, Ford PC. FTIR and optical spectroscopic studies of the reactions of heme models with nitric oxide and other NOx in porous layered solids. Coord Chem Rev. 2008; 252:1486–1496.
44. Lehnert N, Scheidt WR, Wolf MW. Structure and bonding in heme-nitrosyl complexes and implications for biology. Struct Bonding (Berlin, Ger). 2013; 154:155–224.
45. Nakamoto, K. Infrared and Raman Spectra of Inorganic and Coordination Compounds, part B. 6th. J Wiley and Sons; New York, NY: 2009. p. Chapter 1
46. Kurtikyan TS, Hovhannisyan AA, Gulyan GM, Ford PC. Interaction of nitrogen bases with iron-porphyrin nitrito complexes Fe(Por)(ONO) in sublimed solids. Inorg Chem. 2007; 46:7024–7031. [PubMed: 17636900]
47. Kurtikyan TS, Ford PC. Reactions of nitrogen oxides with heme models: spectral characterization of an elusive five-coordinate FeIII(porphyrin) nitrito intermediate. Angew Chem, Int Ed. 2006; 45:492–496.
48. Irish DE, Thorpe RV. Raman spectral studies of cadmium-nitrite interactions in aqueous solutions and crystals. Can J Chem. 1975; 53:1414–1423.
49. Ianoul A, Coleman T, Asher SA. UV resonance Raman spectroscopic detection of nitrate and nitrite in wastewater treatment processes. Anal Chem. 2002; 74:1458–1461. [PubMed: 11922318]
50. Zafiriou OC, Bonneau R. Wavelength-dependent quantum yield of OH radical formation from photolysis of nirite ion in water. Photochem Photobiol. 1987; 45:723–727.
51. Jankowski JJ, Kieber DJ, Mopper K. Nitrate and nitrite ultraviolet actinometers. Photochem Photobiol. 1999; 70:319–328.
52. Nakamoto K, Fujita J, Murata H. Infrared spectra of metallic complexes. V. The infrared spectra of nitro and nitrito complexes. J Am Chem Soc. 1958; 80:4817–4823.
53. Lehnert N, Cornelissen U, Neese F, Ono T, Noguchi Y, Okamoto K, Fujisawa K. Synthesis and spectroscopic characterization of copper(II)-nitrito complexes with hydrotris(pyrazoyl)borate and related coligands. Inorg Chem. 2007; 46:3916–3933. [PubMed: 17447754]
54. Yi J, Richter-Addo GB. Unveiling the three-dimensional structure of the green pigment of nitrite-cured meat. Chem Commun. 2012; 48:4172–4174.
55. Wojciechowski G, Ortiz de Montellano PR. Radical energies and the regiochemistry of addition to heme groups. Methylperoxy and nitrite radical additions to the heme of horseradish peroxidase. J Am Chem Soc. 2007; 129:1663–1672. [PubMed: 17249668]
56. Olson JS, Phillips GN Jr. Myoglobin discriminates between O_2, NO and CO by electrostatic interactions with the bound ligand. J Biol Inorg Chem. 1997; 2:544–552.

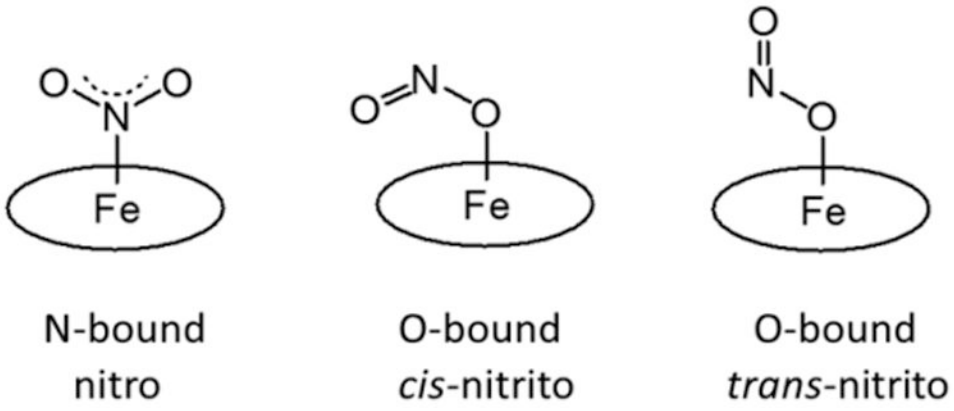

Figure 1.
Heme-nitrite linkage isomers.

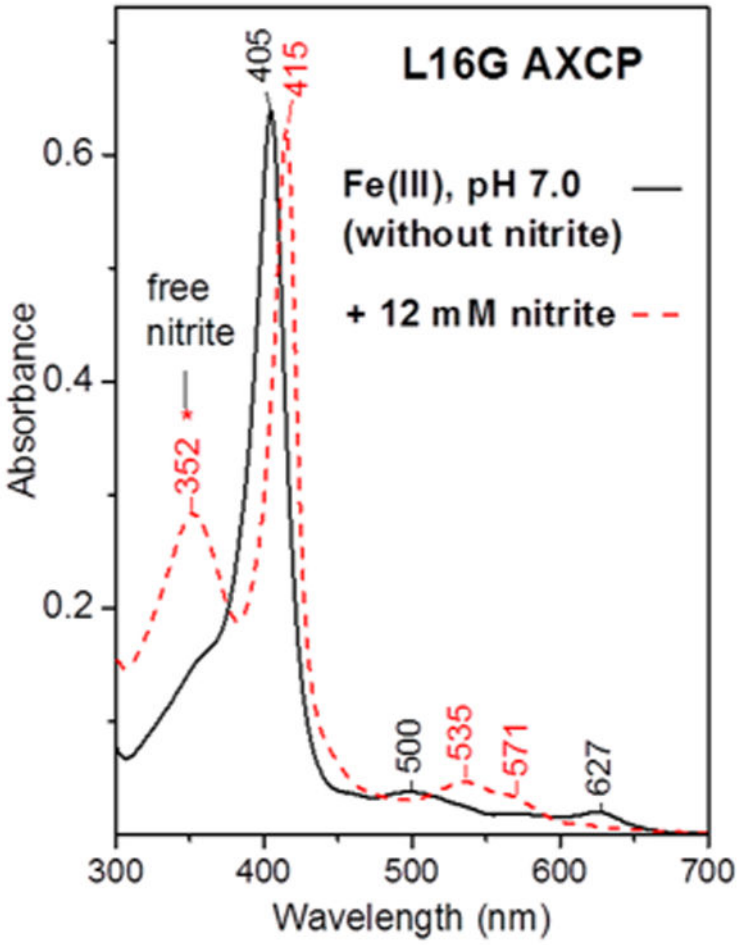

Figure 2.
Effect of nitrite on the UV-visible absorption spectrum of Fe(III) L16G AXCP.

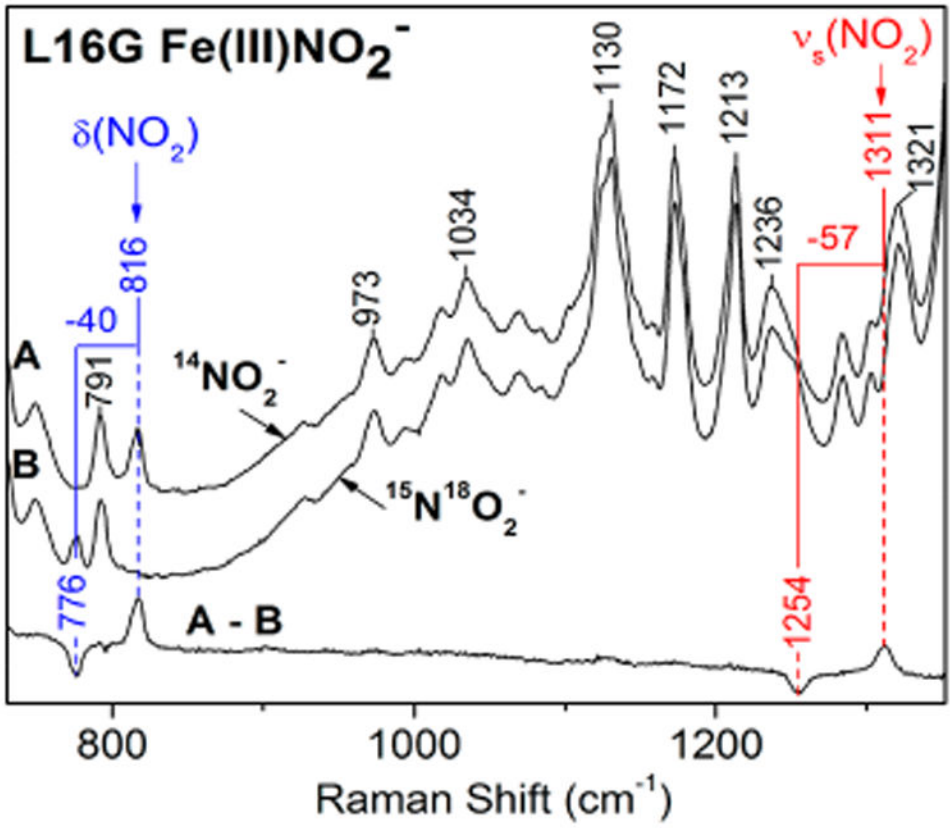

Figure 3.

Midfrequency RR region of Fe(III)-nitrite L16G AXCP showing the identification of $\delta(NO_2)$ and $\nu_s(NO_2)$ vibrations via substitution with $^{15}N^{18}O_2^-$.

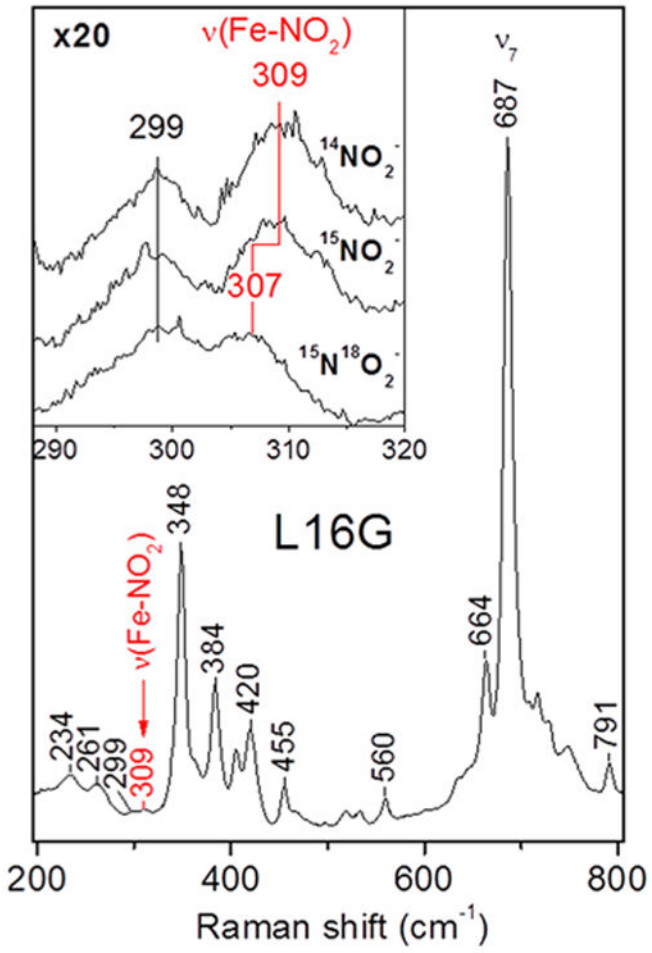

Figure 4.

Low frequency RR spectrum of Fe(III)-nitrite L16G AXCP. Inset shows the identification of the ν(Fe–NO_2) vibration via isotopic substitution. Isotope data for the ~400–800 cm^{-1} region is shown in Figure S7).

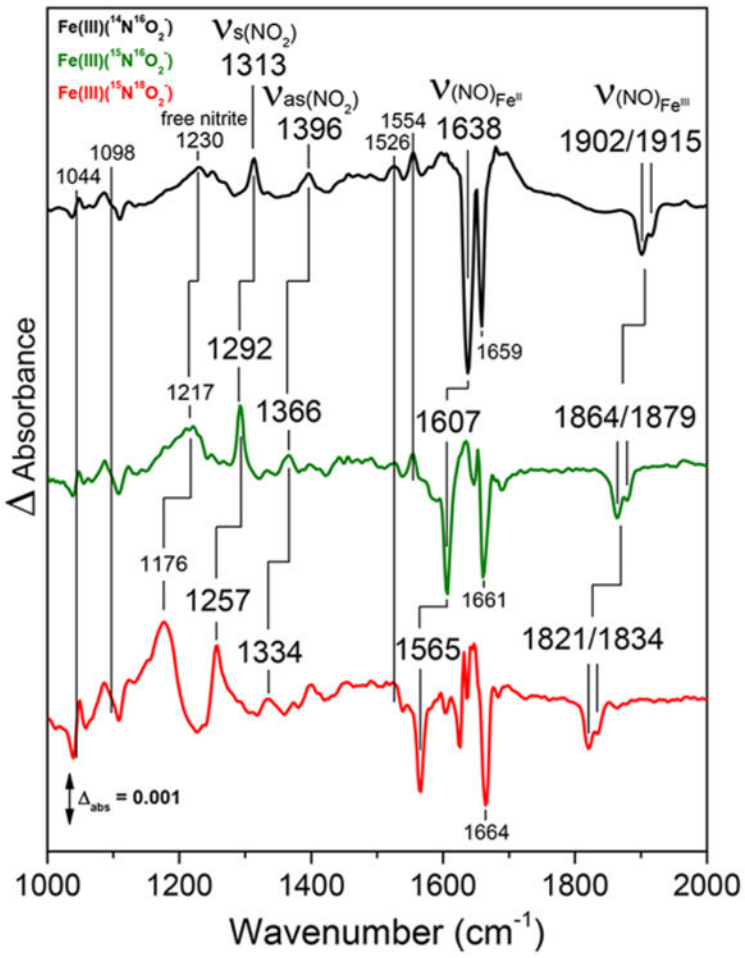

Figure 5.

Room-temperature FTIR difference spectra obtained after illumination of L16G Fe(III)-nitrite complexes with 351 nm.

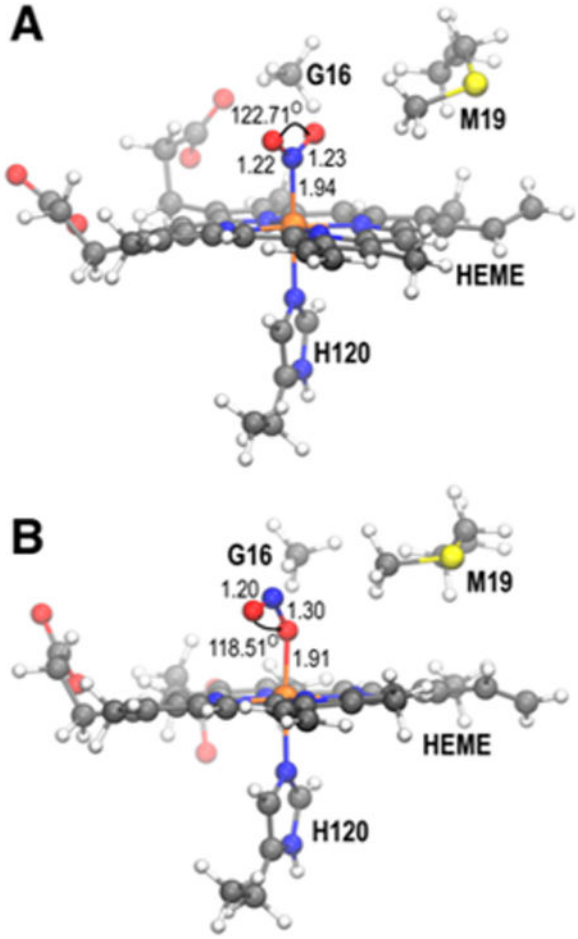

Figure 6.

Optimized structures of the L16G AXCP Fe(III)-nitrite complex showing (A) nitro and (B) nitrito coordination modes. Note: His120, Gly16, and Met19 residues are truncated at Cα carbons as CH_3 groups.

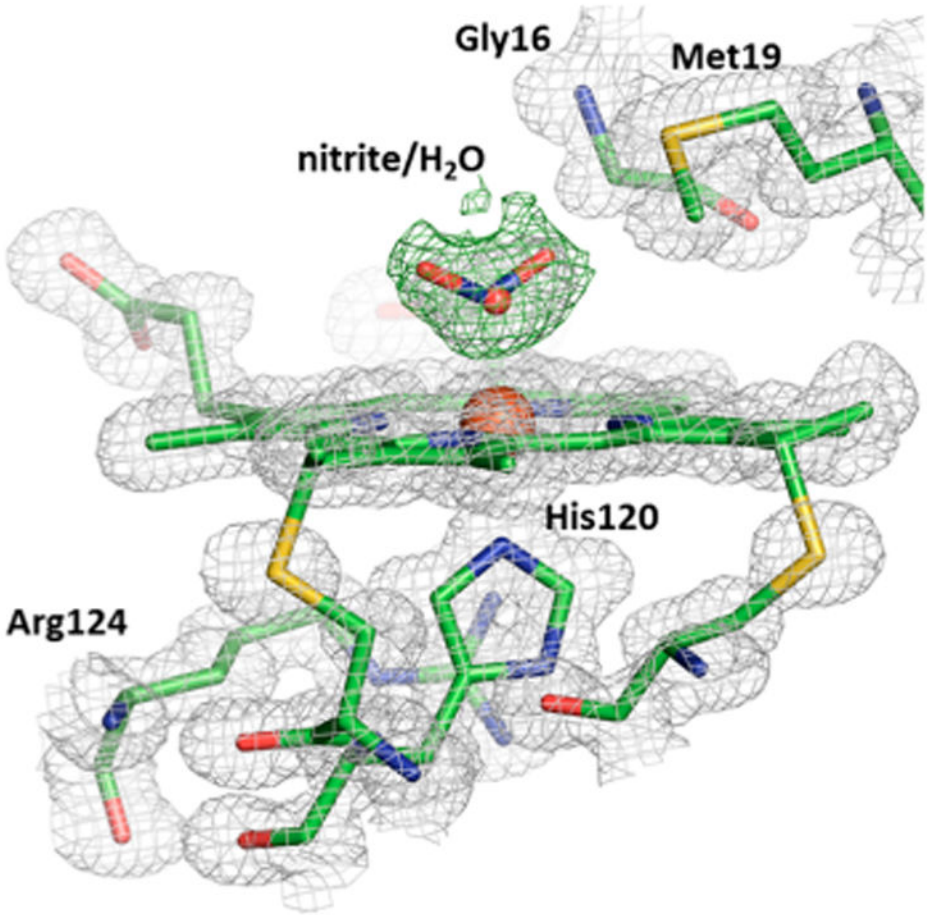

Figure 7.

Low-dose (0.16 MGy) X-ray crystal structure of the heme environment of L16G-nitrite AXCP at 1.06 Å resolution showing a weighted electron density F_o-F_c omit map (green) superimposed on the $2F_o$-F_c map (gray) contoured at 0.44 e/Å^3. A mixture of nitrite and water were modeled as heme ligands in the proportion 0.25:0.75 to account for the ligand electron density with B-factors 19.6/17.8/19.7 Å^2 for nitrite O/N/O atoms, 10.4 Å^2 for water, and 8.9 Å^2 for the Fe atom. The Fe–N(nitrite) distance is 2.1 Å, Fe–N–O angles 118°/120°, and Fe-water distance 2.07 Å.

Table 1

Vibrational Frequencies (in cm^{-1}) of Fe(III)-Porphyrin-Nitrite Complexes and Other Nitrite Species[a]

nitrite species	$\nu_{as}(NO_2)$ or ν(N=O)	$\nu_s(NO_2)$ or ν(N–O)	$\delta(NO_2)$ or δ(ONO)	ν(Fe-NO_2) or ν(Fe-ONO)	ref
6c Nitro					
L16G AXCP (exptl)	1396 (−30, −62)	1311 (−21, −57)	816 (−7, −40)	309 (~0, −2)	tw
L16G AXCP (calcd)	1588 (−31, −69)	1428 (−23, −65)	849 (−8, −43)	318 (~0, −1)	tw
Fe(TTP)(1-MeIm)(NO_2)	1396 (−33)	1312 (−21)	813 (−7)	nd	46
Fe(TTP)(NH_3)(NO_2)	1401 (−34)	1312 (−21)	810 (−6)	nd	46
Fe(TTP)(py)(NO_2)	1405 (−32)	1306 (−19)	810 (−6)	nd	46
HRP	nd	1272 (−32, −54)	822 (−7, −44/−24)	563 (−19, −23)	27
6c Nitrito					
Fe(TTP)(NH_3)(ONO)	*1470 (−32)*	*969 (−17)*	*~827 (−5)*	nd	46
Mb	*1470 (−35, −70)*	*998 (−28, −44)*	*818 (−20, −28)*	*296/256 (0, −18)*	24, 26
L16G AXCP (calcd)	*1608 (−20, −73)*	*1094 (−22, −47)*	*886 (−4, −48)*	*328 (~0, −2)*	tw
5c Nitrito					
Fe(TTP)(ONO)	*1528 (−34)*	*902 (−23)*	*751 (−4)*	nd	47
Nitrovinyl					
HRP	nd	1334 (−25, −55)	nd		27
Mb	1518 (−36)	1324 (−20)	nd		24, 26
Free Nitrite					
$NO_2^{-}{}_{(aq)}$	~1240	1325–1331	817		48, 49

[a] Data in italics refer to nitrito vibrations. Values in parentheses indicate frequency shifts upon substitution with $^{15}NO_2^-$ and $^{15}N^{18}O_2^-$. Abbreviations: tw, this work; nd, not determined.